OPEN ACCESS



Eight New Substellar Hyades Candidates from the UKIRT Hemisphere Survey

Adam C. Schneider , Michael C. Cushing , Robert A. Stiller , Jeffrey A. Munn , Frederick J. Vrba , Justice Bruursema , Stephen J. Williams , Michael C. Liu , Alexia Bravo , Jacqueline K. Faherty , Austin Rothermich , Emily Calamari , Dan Caselden , Martin Kabatnik , Arttu Sainio , Thomas P. Bickle , William Pendrill , Nikolaj Stevnbak Andersen , and Melina Thévenot , and Melina Thévenot

⁶ School of Physical Sciences, The Open University, Milton Keynes, MK7 6AA, UK Received 2024 July 19; revised 2024 August 16; accepted 2024 August 18; published 2024 September 20

Abstract

We have used the UKIRT Hemisphere Survey combined with the UKIDSS Galactic Cluster Survey, the UKIDSS Galactic Plane Survey, and the CatWISE2020 catalog to search for new substellar members of the nearest open cluster to the Sun, the Hyades. Eight new substellar Hyades candidate members were identified and observed with the Gemini/GNIRS near-infrared spectrograph. All eight objects are confirmed as brown dwarfs with spectral types ranging from L6 to T5, with two objects showing signs of spectral binarity and/or variability. A kinematic analysis demonstrates that all eight new discoveries likely belong to the Hyades cluster, with future radial velocity and parallax measurements needed to confirm their membership. CWISE J042356.23+130414.3, with a spectral type of T5, would be the coldest ($T_{\rm eff} \approx 1100~{\rm K}$) and lowest-mass ($M \approx 30~M_{\rm Jup}$) free-floating member of the Hyades yet discovered. We further find that high-probability substellar Hyades members from this work and previous studies have redder near-infrared colors than field-age brown dwarfs, potentially due to lower surface gravities and supersolar metallicities.

Unified Astronomy Thesaurus concepts: L dwarfs (894); T dwarfs (1679); Brown dwarfs (185); Open star clusters (1160)

1. Introduction

As a cluster containing several naked-eye stars, the Hyades has been known since prehistory. The first instance of the Hyades cluster having been cataloged was likely in G. B. Hodierna (1654), where it was labeled as a "Luminosae," or a region containing stars visible to the naked eye. Compilations of Hyades members did not occur in earnest until the emergence of proper motion measurements, with the first recognition that some stars in the area of the Hyades may share similar proper motions (and thus be physically associated) noted in R. A. Proctor (1870). Early compilations (e.g., C. W. Wirtz 1902; F. Kustner 1902; H. A. Weersman 1904; J. C. Kapteyn & W. Desetter 1904) presented some of the first proper motion measurements in this area of the sky and cataloged dozens of members, with C. W. Wirtz (1902) likely showing the first map of the Hyades in a scientific journal. It was not until the pioneering work of L. J. Boss (1908) where it was shown that the proper motion vectors of many proposed members were converging toward a single point in the sky, solidifying the physical association of many cluster members. Further studies continued to expand the number and properties of stellar Hyades members based on astrometric and photometric measurements (e.g., E. Hertzsprung 1921; P. J. van Rhijn & J. J. Raimond 1934; J. Titus & W. W. Morgan 1940; J. M. Ramberg 1941; R. E. Wilson 1948; H. G. van Bueren 1952; H. L. Johnson & C. F. Knuckles 1955; H. L. Giclas et al. 1962; G. Pels et al. 1975;

Original content from this work may be used under the terms of the Creative Commons Attribution 4.0 licence. Any further distribution of this work must maintain attribution to the author(s) and the title of the work, journal citation and DOI.

R. B. Hanson 1975; A. R. Upgren & E. W. Weis 1977; J. H. Oort 1979; M. A. C. Perryman et al. 1998; J. H. J. de Bruijne et al. 2001; S. Röser et al. 2011; S. Reino et al. 2018; S. Meingast & J. Alves 2019; S. Röser et al. 2019). Such efforts to fill out the census of Hyades stars were complemented with targeted searches for fainter, lower-mass members (e.g., A. van Maanen 1942; W. J. Luyten & P. W. Merrill 1954; G. H. Herbig 1962; W. F. van Altena 1966; P. Pesch 1968; W. F. van Altena 1969; J. Stauffer 1982; B. Zuckerman & E. E. Becklin 1987; S. K. Leggett & M. R. S. Hawkins 1989; C. Bryja et al. 1992; N. Reid 1992, 1993; C. Bryja et al. 1994; J. R. Stauffer et al. 1994; S. K. Leggett et al. 1994; J. R. Stauffer et al. 1995; I. N. Reid & J. E. Gizis 1997; H. C. Harris et al. 1999; I. N. Reid & S. L. Hawley 1999; J. E. Gizis et al. 1999; I. N. Reid & S. Mahoney 2000; P. D. Dobbie et al. 2002; N. P. Bannister & R. F. Jameson 2007; E. Hogan et al. 2008; J. Bouvier et al. 2008; B. Goldman et al. 2013; N. Lodieu et al. 2014; S. L. Casewell et al. 2014; A. Pérez-Garrido et al. 2017, 2018; S. Melnikov & J. Eislöffel 2018; N. Lodieu et al. 2019; Z. Zhang et al. 2021; A. C. Schneider et al.

Brown dwarfs, substellar objects that have masses below the hydrogen burning minimum mass ($M \lesssim 0.075 \, M_{\odot}$) and cannot sustain hydrogen fusion in their cores (C. Hayashi & T. Nakano 1963; S. S. Kumar 1963), have been historically challenging to find in the Hyades. The main obstacles that arise when investigating the Hyades population below the stellar boundary are the cluster's large spatial extent on the sky and the intrinsic faintness of substellar objects at the distance of the Hyades (~ 47 pc; Gaia Collaboration et al. 2021). Despite these hurdles, several substellar members of the Hyades have been

United States Naval Observatory, Flagstaff Station, 10391 West Naval Observatory Rd., Flagstaff, AZ 86005, USA; adam.c.schneider4.civ@us.navy.mil Ritter Astrophysical Research Center, Department of Physics and Astronomy, University of Toledo, 2801 W. Bancroft St., Toledo, OH 43606, USA Institute for Astronomy, University of Hawaii at Manoa, Honolulu, HI 96822, USA

⁴ Department of Astrophysics, American Museum of Natural History, Central Park West at 79th St., New York, NY 10024, USA
⁵ Backyard Worlds: Planet 9, USA

identified, either by focusing on an area smaller than the full extent of the cluster core (e.g., E. Hogan et al. 2008; J. Bouvier et al. 2008), conducting shallow (but wide) investigations that detected some of the nearest substellar members (e.g., A. Pérez-Garrido et al. 2017, 2018), performing high-contrast imaging to detect substellar companions to known stellar members (M. Kuzuhara et al. 2022; K. Franson et al. 2023), or complete serendipity (e.g., A. C. Schneider et al. 2017, 2023).

Any such discoveries, however, hold incredible value as benchmark systems. As one of the most well-studied clusters, the Hyades has an established age (\sim 650 Myr; Y. Lebreton et al. 2001; S. De Gennaro et al. 2009; E. L. Martín et al. 2018; S. Gossage et al. 2018; N. Lodieu et al. 2019; N. Lodieu 2020). Models that include rotation predict a slightly older age for the Hyades cluster (750 ± 100 Myr; T. D. Brandt & C. X. Huang 2015a, 2015b), however these ages are in tension with previous estimates and more recent determinations using the lithium depletion boundary (e.g., E. L. Martín et al. 2018; N. Lodieu 2020) and white dwarfs (N. Lodieu et al. 2019). The Hyades also has a well-determined metallicity ([Fe/H] \sim 0.15 dex; J. D. Cummings et al. 2017). Such properties are exceptionally difficult to determine for solitary brown dwarfs not belonging to a known association.

While the spatial extent of the Hyades presents a challenge to its exploration, the proper motion of the cluster (~100 mas yr⁻¹) provides a significant advantage for distinguishing candidate substellar members from the myriad of background sources. Using new proper motion measurements, A. C. Schneider et al. (2022) performed a large area search for new candidate substellar members of the Hyades using the UKIRT Hemisphere Survey (UHS; S. Dye et al. 2018), which reaches ~4 mag deeper than the Two Micron All-Sky Survey (2MASS; M. F. Skrutskie et al. 2006). Candidates were found by combining UHS with the CatWISE2020 catalog (F. Marocco et al. 2021), both of which cover the majority of the spatial extent of the Hyades.

In this work, we have expanded the search of A. C. Schneider et al. (2022), probing deeper in the cluster and to colder temperatures, identifying eight candidates with colors consistent with known field late-L or T dwarfs and motions consistent with Hyades membership. In Section 2 we describe the target selection for these new substellar Hyades candidates. In Section 3 we describe our follow-up spectroscopic observations. In Section 4 we analyze the characteristics of each new candidate, including spectral types, distance estimates, Hyades membership, and physical properties. Finally in Section 5 we discuss the near-infrared colors of the current census of substellar Hyades members compared to those of the field-age brown dwarf population, and summarize our results in Section 6.

2. Target Selection

We use a similar candidate selection strategy as in A. C. Schneider et al. (2022) with a few key differences. A. C. Schneider et al. (2022) searched for substellar Hyades candidates using the UHS and CatWISE2020 catalogs, limiting new candidates to those having *J*-band magnitudes brighter than 17.5 mag. This limit was imposed such that a spectrum with a reasonable signal-to-noise (S/N) could be obtained with the SpeX spectrograph on the 3 m IRTF telescope. For this current search, we have increased the *J*-band magnitude limit to 18 mag. This magnitude limit was chosen to focus on the brightest new candidates. Deeper searches for candidates are

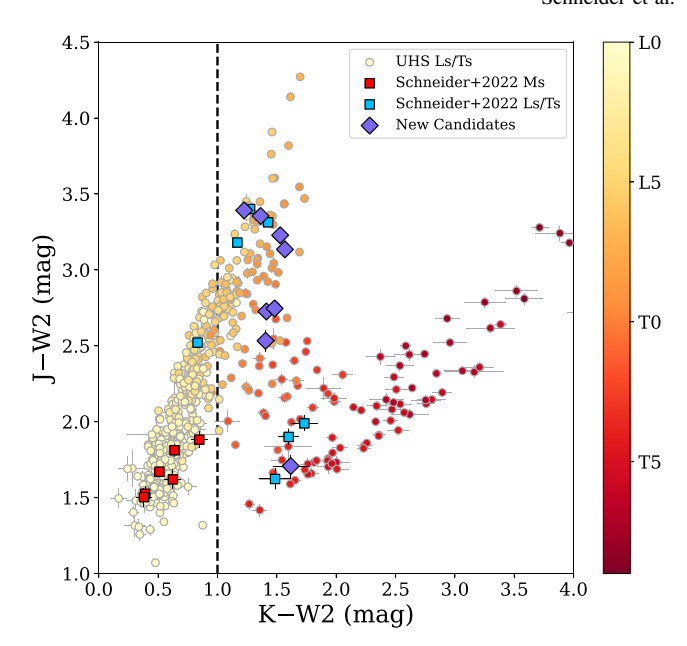


Figure 1. J-W2 vs. K-W2 colors for known L and T dwarfs from the UKIRT Hemisphere Survey (A. C. Schneider et al. 2023) compared to discoveries from A. C. Schneider et al. (2022) and new candidates presented in this work. Note that the color cut requiring new candidates have K-W2 colors greater than 1.0 mag effectively eliminates the late-M-type objects that contaminated the A. C. Schneider et al. (2022) sample.

feasible, as UHS has a *J*-band 5σ limiting magnitude of 19.6 (S. Dye et al. 2018). We also include detections in previous UKIDSS surveys (A. Lawrence et al. 2007) combined with UHS to determine proper motions of new candidates, extending the time baseline for proper motion measurements from \sim 5 to \sim 10 yr. Following the methods described in A. C. Schneider et al. (2023), we recalibrate the position of each UKIRT detection for each source using the Gaia DR3 (Gaia Collaboration et al. 2023) reference frame.

Following A. C. Schneider et al. (2022), we have limited our search to objects that are within 18 pc of the Hyades cluster center, which should include all bound and halo cluster members (N. Lodieu et al. 2019). Candidates were chosen to also have colors consistent with late-L and T dwarfs. Specifically, we chose objects with J-W2 colors greater than 1.5 mag and K-W2 colors greater than 1.0 mag. The first color requirement selects red, late-type (\gtrsim M7) objects, while the second color criterion effectively filters out late-M dwarfs, such as those that contaminated the A. C. Schneider et al. (2022) sample. Our color selection criteria is illustrated in Figure 1.

To ensure each candidate has proper motion components consistent with known Hyades members from the Gaia Catalog of Nearby Stars (Gaia Collaboration et al. 2021), we verified each source is a kinematic match to the Hyades central cluster using the BANYAN Σ classifier (J. Gagné et al. 2018) and a convergent point analysis (e.g., A. C. Schneider et al. 2022). Specifically, we required that the BANYAN Σ probability of Hyades membership using positions and measured proper motions to be greater than 0%. We chose this conservative value to ensure no potential candidates are missed, however we note that most of our final candidates have BANYAN Σ probabilities \geqslant 80%. For the convergent point analysis, we required the proper motion angle ($\theta_{\rm cp}$), defined as the angle between a line pointing north and a line from each candidate pointed to the convergent point,

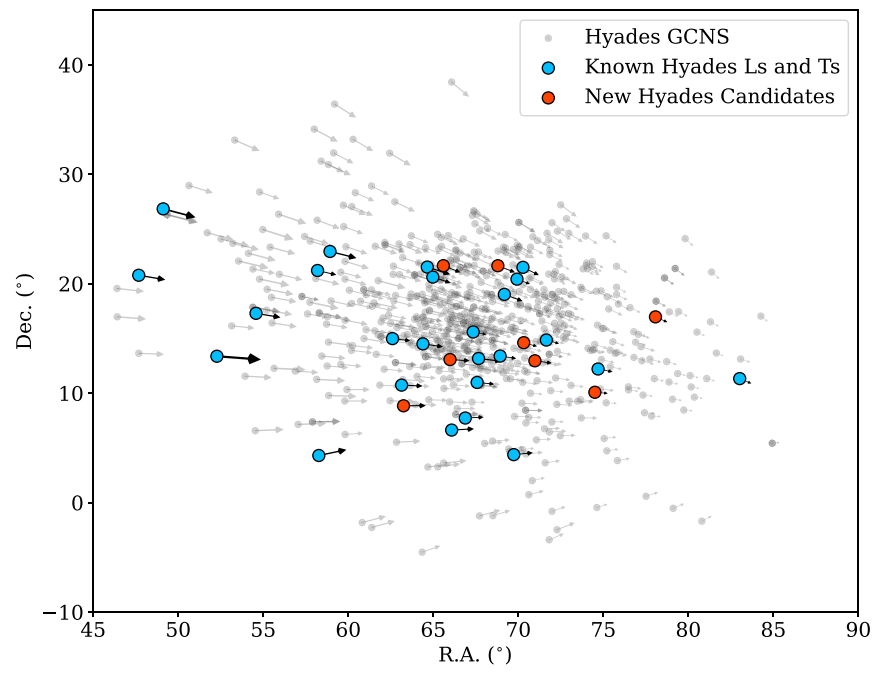


Figure 2. The positions and proper motion vectors of our new substellar Hyades candidates (red) and known L and T type candidate members of the Hyades (blue; A. C. Schneider et al. 2022) compared to all known Hyades members (gray) within the halo radius (18 pc) from the Gaia Catalog of Nearby Stars (Gaia Collaboration et al. 2021).

to be within 7° of each other $(\sim 3\sigma)$. This search revealed several new substellar Hyades candidate members. This work focuses on the eight brightest new candidates ($J \le 18$ mag). The positions and proper motion vectors of these candidates compared to known Hyades members are shown in Figure 2.

Of the eight candidates discussed in this work, seven were imaged by previous UKIRT Surveys, either in the UKIDSS Galactic Plane Survey (GPS; P. W. Lucas et al. 2008) or Galactic Cluster Survey (GCS; A. Lawrence et al. 2007). Two of the candidates were found in both the GCS and GPS (CWISE J042222.17+213900.5 and CWISE J043511.26 +213846.3). CWISE J044354.22+125736.7 has an available UKIDSS GCS K-band image, but has no matching entries in the UKIDSS GCS catalog. For this image, we use the imcore routine from the CASUTOOLS package⁷ (M. J. Irwin et al. 2004) to extract source positions and photometry. We recalibrate these extracted positions in the same method as the other survey images and provide the position of this source from the UKIDSS GCS K-band image in Table 1. Offsets between catalog positions and our recalibrations for all eight candidates were between 16 mas and 163 mas, with an average offset of 92 mas.

The proper motions and photometric measurements of the eight new candidates are listed in Table 2. We include photometry from CatWISE2020 (F. Marocco et al. 2021), UHS (S. Dye et al. 2018), and Pan-STARRS1 (PS1) DR2 (K. C. Chambers et al. 2016; E. A. Magnier et al. 2020). Several of these sources were independently identified as candidate brown dwarfs through the Backyard Worlds: Planet 9 citizen science project (M. J. Kuchner et al. 2017). These volunteers are credited as codiscoverers and noted in Table 2.

3. Observations

All eight substellar Hyades candidates were observed with the Gemini Near-InfraRed Spectrograph (GNIRS; J. H. Elias et al. 2006) at the Gemini North Telescope in November 2023 (PID: GN-2023B-Q-316). GNIRS was operated in the non-AO cross-dispersed mode with the 1" slit and the 32 1/mm grating ($R = 500, 0.8-2.5 \mu m$). Each target was dithered between two positions along the slit separated by 3" in an ABBA pattern. A summary of the observations is given in Table 3. This table includes the total exposure time and the S/N per pixel at the *J*-band peak between 1.27 and 1.29 μm .

All spectra were reduced with the open-source Python package PypeIt (J. Prochaska et al. 2020; J. X. Prochaska et al. 2023). PypeIt performs flat-fielding, wavelength calibration, flux calibration, and telluric corrections. The reduced spectra are shown in Figure 3.

4. Analysis

4.1. Spectral Types

Spectral types for each source were determined by comparing the observed spectra to L and T dwarf near-infrared spectral standards from A. J. Burgasser et al. (2006a) and J. D. Kirkpatrick et al. (2010). The best-fit spectral types were determined by finding the minimum χ^2 values comparing the *J*-band portion of each spectrum (1.0–1.35 μ m) to each spectral standard. The best-fit types are given in Table 3 and comparisons to the best-fitting standards are shown in Figure 3. Additional notes on individual spectra are given in the following subsections.

4.1.1. CWISE J043511.26+213846.3, CWISE J051215.86+165818.0, CWISE J044116.07+143645.4, and CWISE J042356.23+130414.3

All four of these objects show reasonably good fits to their respective best-matching standards. Of these, CWISE J042356.23+130414.3 is particularly noteworthy with a T5

http://casu.ast.cam.ac.uk/surveys-projects/software-release

Table 1
Astrometric Measurements^a

CWISE	R.A.	R.A. err	Decl.	Decl. err	Epoch	Survey
Name	(°)	(mas)	(°)	(mas)	(year)	
J041259.89+085049.6	63.249233276	24.2843	8.847085790	25.5046	2006.0119	GCS (K)
	63.249487662	23.7192	8.847089852	24.7934	2013.1109	UHS (J)
	63.249729257	13.3274	8.847090340	13.7931	2018.8528	UHS (K)
J042222.17+213900.5	65.592092834	23.6696	21.650238453	21.1248	2005.7772	GCS(K)
	65.592082447	27.6446	21.650231543	28.5865	2005.9108	GPS(J)
	65.592096152	19.8400	21.650230210	19.6598	2005.9108	GPS (H)
	65.592088999	21.2632	21.650231288	22.7655	2005.9108	GPS(K)
	65.592338488	19.9523	21.650140765	19.2822	2013.9792	UHS (J)
	65.592478643	13.9178	21.650092527	11.0290	2018.0148	UHS (K)
J042356.23+130414.3	65.983999636	95.7351	13.070798587	95.0150	2005.7798	GCS(K)
	65.984283283	13.7973	13.070763288	13.7151	2013.9002	UHS (J)
	65.984426861	46.6846	13.070765354	46.7912	2018.1185	UHS (K)
J043511.26+213846.3	68.796669723	24.3706	21.646361000	22.7210	2005.7773	GCS(K)
	68.796659215	23.7114	21.646367350	23.2133	2005.8866	GPS(J)
	68.796661991	20.1629	21.646368124	18.9891	2005.8866	GPS (H)
	68.796652499	32.7252	21.646357953	36.6166	2005.8866	GPS(K)
	68.796951296	13.3308	21.646258961	13.0415	2015.0361	UHS (J)
	68.797045604	13.8996	21.646234299	14.6700	2017.9273	UHS (K)
	68.797077425	16.0486	21.646206952	16.8108	2018.7874	UHS (K)
J044116.07+143645.4	70.316806464	66.7943	14.612599107	67.3614	2005.7799	GCS(K)
	70.317022493	40.0415	14.612538522	39.5753	2015.0302	UHS (J)
	70.317071886	36.3958	14.612505110	34.7169	2016.5561	UHS (J)
	70.317067518	34.4074	14.612531056	34.6010	2016.9034	UHS (J)
	70.317091733	21.2303	14.612524547	21.6415	2017.8672	UHS (K)
J044354.22+125736.7	70.975750977	19.6853	12.960214359	19.6748	2009.6828	GCS(K)
	70.975908997	17.5431	12.960198900	17.4367	2014.9459	UHS (J)
	70.975998969	19.6072	12.960185199	18.4786	2017.8670	UHS (K)
	70.975998431	15.1848	12.960177469	14.8130	2018.0502	UHS (K)
J045800.69+100456.9	74.502673652	44.1223	10.082517681	43.8587	2005.8727	GCS(K)
	74.502889253	18.1274	10.082491683	17.4784	2014.9405	UHS (J)
	74.502943664	21.2104	10.082496415	20.9111	2017.8427	UHS (K)
J051215.86+165818.0	78.066057176	18.8927	16.971622726	17.5606	2013.0839	UHS (J)
	78.066171159	17.2959	16.971585306	17.9962	2018.0065	UHS (K)
	78.066150641	24.5892	16.971566542	25.461	2018.0175	UHS (K)

Note.

spectral type. If confirmed as a Hyades member, CWISE J042356.23+130414.3 would have the latest spectral type among Hyades free-floating Hyades members.

4.1.2. CWISE J042222.17+213900.5

CWISE J042222.17+213900.5 is unusually red compared to the L6 spectral standard. Figure 4 shows that this object is a very good match spectroscopically to WISEA J020047.29 -510521.4 (A. C. Schneider et al. 2017). A. C. Schneider et al. (2017) suggested WISEA J020047.29-510521.4 as a probable AB Dor member ($\sim\!150$ Myr; C. P. M. Bell et al. 2015). Using updated astrometry of this source from J. D. Kirkpatrick et al. (2021), which includes proper motion components $\sim\!5\times$ more precise than the proper motion previously used to evaluate moving group membership and a measured parallax, we find a 99.5% probability of belonging to AB Dor using BANYAN Σ (J. Gagné et al. 2018).

Unusually red colors are often associated with low-surface gravity, though there are exceptions (e.g., F. Marocco et al. 2014). We evaluated the surface gravity of CWISE J042222.17 +213900.5 using the K. N. Allers & M. C. Liu (2013) spectral indices that are applicable to objects with spectral types of L6 (FeH_J and H-cont). We find values of 1.17 and 0.87 for FeH_J

and H-cont, respectively, which indicates a normal field gravity according to K. N. Allers & M. C. Liu (2013). We also evaluated the $H_2(K)$ index (J. I. Canty et al. 2013; A. C. Schneider et al. 2014), and again find a value (1.12) consistent with the field population. This suggests that while CWISE J042222.17+213900.5 is unusually red, it does not have a surface gravity low enough to distinguish it from the field population. WISEA J020047.29-510521.4, on the other hand, has FeH $_J$, H-cont, and $H_2(K)$ values (1.06, 0.90, and 1.07, respectively) that suggest low to intermediate surface gravity, as expected for an AB Dor member. Thus, while the overall spectral shape of CWISE J042222.17+213900.5 and WISEA J020047.29-510521.4 are similar, the gravity sensitive regions show that the surface gravities of these two sources are distinct.

4.1.3. CWISE J044354.22+125736.7

CWISE J044354.22+125736.7 most closely matches the L9 standard at J, but is not a great fit elsewhere. We note that this is the lowest-S/N spectrum presented in this work, and a higher-S/N spectrum may be needed for a more accurate classification.

^a All positions and uncertainties are determined by astrometrically recalibrating UHS and UKIDSS positions using the Gaia DR3 reference frame.

5

Table 2 New Substellar Hyades Candidates

CWISE Name	μ_{α} (mas yr ⁻¹)	$(ext{mas yr}^{-1})$	z _{PS1} (mag)	y _{PS1} (mag)	$J_{ m UHS}$ (mag)	K _{UHS} (mag)	W1 (mag)	W2 (mag)
J041259.89+085049.6a	138.20 ± 2.58	1.21 ± 2.69	21.223 ± 0.017	19.706 ± 0.153	17.530 ± 0.044	16.216 ± 0.040	15.460 ± 0.022	14.804 ± 0.025
J042222.17+213900.5 ^b	106.13 ± 1.87	-41.57 ± 1.61	20.939 ± 0.152	20.028 ± 0.279	17.712 ± 0.042	15.545 ± 0.023	14.709 ± 0.017	14.320 ± 0.019
J042356.23+130414.3	120.96 ± 8.36	-7.19 ± 8.34		20.145 ± 0.090	17.651 ± 0.032	17.560 ± 0.136	17.138 ± 0.062	15.943 ± 0.067
J043511.26+213846.3°	106.80 ± 1.55	-41.49 ± 1.54	20.864 ± 0.043	20.076 ± 0.022	17.894 ± 0.043	15.902 ± 0.032	14.998 ± 0.019	14.539 ± 0.023
J044116.07+143645.4	82.64 ± 6.18	-22.91 ± 6.24	20.733 ± 0.047	20.149 ± 0.190	17.932 ± 0.056	16.804 ± 0.061	16.078 ± 0.029	15.399 ± 0.042
J044354.22+125736.7 ^d	104.76 ± 3.57	-14.84 ± 3.51	20.927 ± 0.173	20.065 ± 0.049	17.981 ± 0.040	16.281 ± 0.038	15.343 ± 0.020	14.753 ± 0.025
J045800.69+100456.9 ^e	80.05 ± 4.62	-6.45 ± 4.55			17.901 ± 0.043	16.636 ± 0.060	15.859 ± 0.027	15.155 ± 0.034
J051215.86+165818.0	73.92 ± 6.47	-32.84 ± 6.49		20.007 ± 0.198	17.698 ± 0.039	16.131 ± 0.042	15.110 ± 0.019	14.563 ± 0.022

Notes.

^a CWISE J041259.89+085049.6 was independently discovered by citizen scientists Melina Thévenot, Arttu Sainio, Sam Goodman, and Martin Kabatnik.

b CWISE J042222.17+213900.5 was independently discovered by citizen scientists Nikolaj Stevnbak Andersen, William Pendrill, and Tom Bickle.

^c CWISE J043511.26+213846.3 was independently discovered by citizen scientists Dan Caselden and Tom Bickle.

d CWISE J044354.22+125736.7 was independently discovered by citizen scientists Dan Caselden, Melina Thévenot, Sam Goodman, and William Pendrill.

^e CWISE J045800.69+100456.9 was independently discovered by citizen scientists Arttu Sainio and Martin Kabatnik.

Table 3GNIRS Observations

CWISE Name	Obs. Date (UT)	Total Exp. Time (s)	A0 Star ^a	Spec. Type	$(S/N)_J^b$
J041259.89+085049.6	2023 Nov 14	2400	HIP 22923	T3pec (red)	11
J042222.17+213900.5	2023 Nov 14	2880	HIP 16095	L5–L7 (red)	16
J042356.23+130414.3	2023 Nov 15	2400	HIP 16095	T5	15
J043511.26+213846.3	2023 Nov 19	4320	HIP 17453	L7.5	16
J044116.07+143645.4	2023 Nov 20	4320	HIP 16095	T2	15
J044354.22+125736.7	2023 Nov 15	2400	HIP 28686	L9pec (red)	9
J045800.69+100456.9	2023 Nov 16	1440	HIP 16095	T2pec (red)	12
J051215.86+165818.0	2023 Nov 19	2400	HIP 29371	L9	18

Notes.

4.1.4. CWISE J041259.89+085049.6 and CWISE J045800.69 +100456.9

The single standard fits to CWISE J041259.89+085049.6 and CWISE J045800.69+100456.9 are relatively poor, with the best-fitting standards providing decent fits at J, but not aligning well beyond $\sim 1.4~\mu m$. Using the methods outlined in A. Bravo et al. (2023), we looked for spectral binary templates that better fit the observed spectra for each of these objects than the spectral standards. The best-fitting binary templates for each of CWISE J041259.89+085049.6 (L7+T2) and CWISE J045800.69+100456.9 (L8+T2) are shown in Figure 5. The binary template fits are clearly better matches to the observed spectra for both objects, as reflected in their much lower χ^2_{ν} values.

However, spectral indices potentially point to variability due to a patchy atmosphere as an alternative explanation. A brown dwarf atmosphere with patches of thick, cold clouds and thinner areas that reveal the deeper, hotter layers can have a spectrum that looks very similar to a spectral binary because it includes the contributions of multiple layers in an atmosphere at different temperatures (e.g., 2MASS J21392676+0220226; A. J. Burgasser et al. 2010; J. Radigan et al. 2012). Using the methods and indices defined in A. J. Burgasser et al. (2002, 2006a, 2010) and D. C. Bardalez Gagliuffi et al. (2014), we compared the measured index values for each of these two sources to the binary index regions from A. J. Burgasser et al. (2010) and variability regions from A. Ashraf et al. (2022). Both CWISE J041259.89+085049.6 and CWISE J045800.69 +100456.9 only satisfy a single binary index criterion from A. J. Burgasser et al. (2010; $H_2O - J/CH_4-K$ versus spectral type). Therefore the index values of these two sources do not even satisfy the threshold to be labeled "weak" spectral binary candidates, which is applied to those objects falling in at least two of the spectral binary index defined regions. However, both objects satisfy all eleven of the variability index criteria defined in A. Ashraf et al. (2022). Thus, variability may be the cause of the spectral peculiarity of these objects. Photometric and/or spectroscopic monitoring, as well as high-resolution imaging, may help to identify the causes of these spectral peculiarities.

4.2. Distances

Photometric distances are determined using the spectral type versus absolute magnitude relations from A. C. Schneider et al. (2023) for L, T, and Y dwarfs with UHS photometry and measured parallaxes. The distances given in Table 4 are the

weighted average of the *J*- and *K*-band distances, which are determined considering photometric uncertainties, a \pm 0.5 spectral subtype uncertainty, and the rms scatter of the polynomial fits. The exceptions are the variability candidates (CWISE J041259.89+085049.6 and CWISE J045800.69+100456.9), the very red CWISE J042222.17+213900.5, and the peculiar CWISE J044354.22+125736.7, for which we use \pm 1 spectral subtype uncertainties.

4.3. Hyades Membership

To evaluate the likelihood of Hyades membership for each candidate, we use the BANYAN Σ (J. Gagné et al. 2018) moving group probability calculator as well as a convergent point analysis. Table 4 summarizes the membership evaluation results. For convergent point assessment, we use the convergent point from S. Madsen et al. (2002) and follow the methods in E. Hogan et al. (2008) and A. C. Schneider et al. (2022). As seen in the table, the predicted distances from BANYAN Σ and the convergent point analysis are generally consistent with our photometric distances estimates. Table 4 also shows that the measured convergent point angles (θ_{cp}) and proper motion angles (θ_{μ}) are consistent to within 4° ($\sim 2\sigma$). The table further provides two BANYAN Σ probabilities, the first using only positions and proper motions, while the second includes photometric distance estimates. We include the BANYAN Σ probability without using the photometric distances in case the photometric distance estimate is inaccurate, as would be the case for spectral binaries. However, we note that all BANYAN Σ probabilities increase when photometric distances are included and are greater than 90% for each candidate member. Considering these high BANYAN Σ probabilities, the consistency between photometric distance estimates and distance predictions if true Hyades members, as well as the small differences between θ_{cp} and θ_{μ} , we suggest that each new candidate is a likely Hyades member. Directly measured distances and radial velocities are still needed, however, to fully confirm Hyades membership.

The success rate of these observations for recovering Hyades candidates is high. We attribute this success rate to several factors: (1) the relatively localized area of the sky we limit to around the core of the Hyades cluster; (2) the lessons learned from A. C. Schneider et al. (2022) regarding effective color cuts to filter out nonbrown dwarf background contaminants; and (3) the preselection based on BANYAN Σ probabilities and convergent point restrictions.

^a The A0 star used for telluric correction.

^b Signal-to-noise determined at the *J*-band peak.

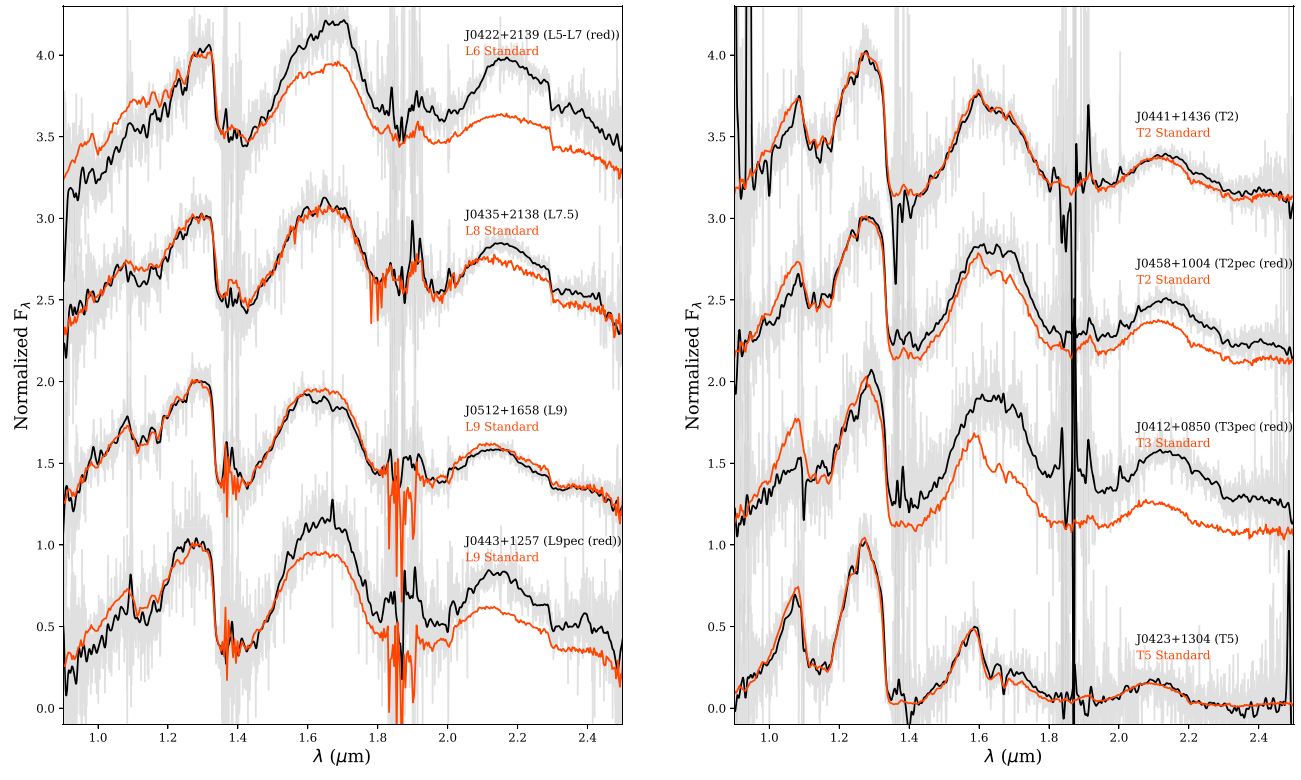


Figure 3. Gemini/GNIRS spectra in full-resolution (gray) and smoothed (black) compared to spectral standards (red–orange). The spectra are normalized between 1.27 and 1.29 μm and offset by integer values for clarity. The spectral standards are: 2MASSI J1010148–040649 (L6; I. N. Reid et al. 2006), 2MASSW J1632291 +190441 (L8; A. J. Burgasser 2007), DENIS-P J0255-4700 (L9; A. J. Burgasser et al. 2006a), SDSSp J125453.90–012247.4 (T2; A. J. Burgasser et al. 2004), 2MASS J12095613–1004008 (T3; A. J. Burgasser et al. 2004), and 2MASS J15031961+2525196 (T5; A. J. Burgasser et al. 2004).

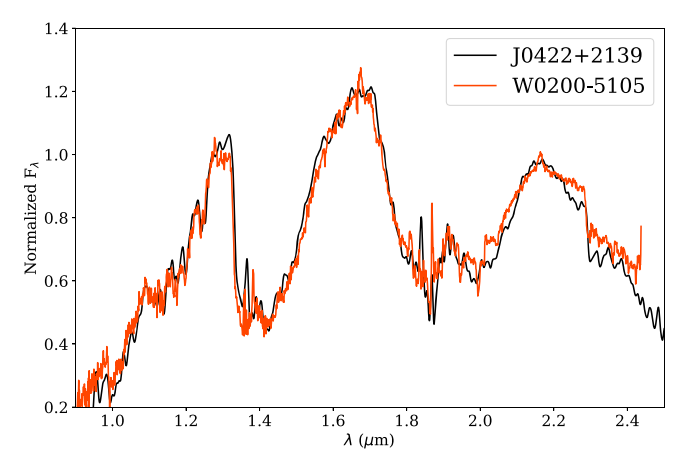


Figure 4. Comparison of the near-infrared spectrum of CWISE J042222.17 +213900.5 to the likely AB Dor member WISEA J020047.29-510521.4 (A. C. Schneider et al. 2017).

4.4. Physical Properties

Brown dwarfs do not form a main sequence, but instead cool and dim over time as they radiate the initial heat of their formation (A. Burrows et al. 1997), which leads to a degenerate relationship between mass, luminosity, and age. Thus, precise fundamental properties of most brown dwarfs are exceptionally difficult to determine. However, if a brown dwarf can be tied to a group of stars with a known age like the Hyades, this degeneracy can be broken. We can therefore estimate the masses of each of our new candidates by using evolutionary models, the age of the Hyades (650 \pm 50 Myr), and effective temperature ($T_{\rm eff}$) estimates derived from spectral types.

In this work, $T_{\rm eff}$ values are estimated using the spectral type versus $T_{\rm eff}$ relation from J. D. Kirkpatrick et al. (2021). All objects are given a ± 0.5 spectral subtype uncertainty, with the exceptions of CWISE J041259.89+085049.6, CWISE J042222.17+213900.5, CWISE J044354.22+125736.7, and CWISE J045800.69+100456.9, for which we assume spectral type uncertainties of \pm 1. $T_{\rm eff}$ values are given in Table 5.

A. C. Schneider et al. (2022) used the evolutionary models of D. Saumon & M. S. Marley (2008) and M. W. Phillips et al. (2020) to estimate the masses of newly discovered objects. In this work, we also use the M. W. Phillips et al. (2020) models, but use the grid that includes the updated equation of state from G. Chabrier et al. (2023). Notably, this updated grid results in slightly higher masses than the previously used M. W. Phillips et al. (2020) evolutionary models. For example, A. C. Schneider et al. (2022) found a mass of $33 \pm 3 M_{\text{Jup}}$ for the T3 brown dwarf Hyades candidate CWISE J043018.70+105857.1 using the M. W. Phillips et al. (2020) models, where we find 35 ± 3 M_{Jup} using M. W. Phillips et al. (2020) models with the updated equation of state. Furthermore, we use the updated Sonora Diamondback evolutionary models of M. S. Marley et al. (2021) and C. V. Morley et al. (2024) instead of D. Saumon & M. S. Marley (2008). We use the solar-metallicity hybrid-grav models in this work, which includes gravity-dependent cloudclearing. Mass estimates assuming Hyades membership are given in Table 5. We note that CWISE J042356.23+130414.3 has the latest spectral type of any free-floating Hyades candidate member, and thus the lowest mass estimates of 33 ± 4 $M_{\rm Jup}$ and 28^{+7}_{-4} $M_{\rm Jup}$ using the M. W. Phillips et al. (2020) and C. V. Morley et al. (2024) models, respectively.

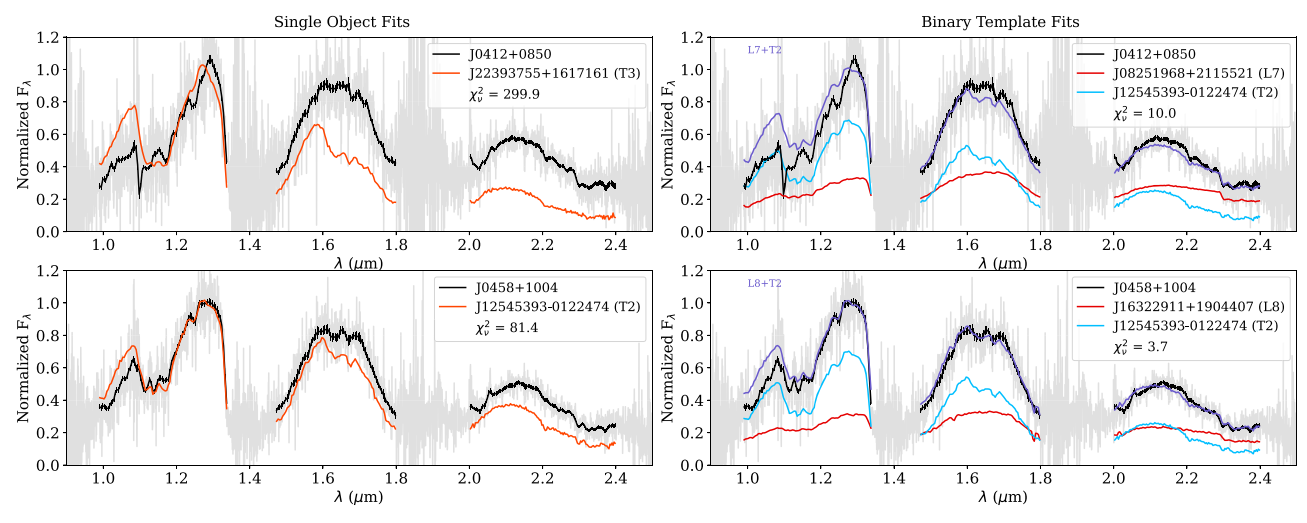


Figure 5. Spectral binary fits for CWISE J041259.89+085049.6 and CWISE J045800.69+100456.9. The individual components used in the fits are 2MASSI J0825196+211552 (L7; J. D. Kirkpatrick et al. 2000; A. J. Burgasser et al. 2010), 2MASSW J1632291+190441 (L8; J. D. Kirkpatrick et al. 1999; A. J. Burgasser 2007), SDSS J125453.90-012247.5 (T2; S. K. Leggett et al. 2000; A. J. Burgasser et al. 2004), and WISEPC J223937.55+161716.2 (T3; J. D. Kirkpatrick et al. 2011).

Table 4
New Hyades Candidate Membership Details

CWISE Name	Spec. Type	dist _{phot} ^a (pc)	dist _{cp} ^a (pc)	dist _{BANYAN} ^a (pc)	θ_{μ}^{b} (°)	$\theta_{\rm cp}^{}$ (°)	BANYAN° (%)	BANYAN ^d (%)
J041259.89+085049.6	T3pec (red)	31 ± 8	39.4	39.1	89.5	90.8	95.9	98.2
J042222.17+213900.5	L5-L7 (red)	54 ± 7	48.1	47.6	111.4	110.9	95.4	97.6
J042356.23+130414.3	T5	38 ± 3	42.2	40.7	94.7	98.2	91.4	98.3
J043511.26+213846.3	L7.5	51 ± 6	44.3	44.6	111.2	113.9	91.1	95.0
J044116.07+143645.4	T2	42 ± 6	53.0	51.1	106.2	103.3	82.4	96.5
J044354.22+125736.7	L9pec (red)	49 ± 5	41.5	41.4	97.8	100.6	93.4	94.7
J045800.69+100456.9	T2pec (red)	41 ± 7	47.3	46.8	95.0	96.2	82.0	97.8
J051215.86+165818.0	L9	44 ± 3	44.1	45.8	114.0	115.8	36.6	90.6

Notes

5. Discussion

While the age of the Hyades is sufficiently old such that many common spectroscopic indicators of youth (e.g., K. N. Allers & M. C. Liu 2013) are indistinguishable from field-age objects for Hyades members, we note that the spectra of both Hyades members in A. C. Schneider et al. (2017) were slightly red compared to spectral standards, while W. M. J. Best et al. (2015) found the L6 Hyades member Hya12 to also be unusually red. Several of the Hyades candidates in this work also appear redder than near-infrared spectral standards (see Figure 3). The distance of the Hyades makes interstellar reddening unlikely to be significant (e.g., B. J. Taylor 2006), and red near-infrared colors are common to young brown dwarfs (e.g., J. K. Faherty et al. 2016; M. C. Liu et al. 2016).

With the new discoveries presented in this work, we can attempt to investigate the near-infrared color sequence for Hyades-age brown dwarfs. Figure 6 shows a J-K versus spectral type diagram comparing high-probability substellar Hyades members (BANYAN $\Sigma \geqslant 80\%$) to field-age brown dwarfs from A. C. Schneider et al. (2023). We use the BANYAN

 Σ probabilities from Table 5 of A. C. Schneider et al. (2022) for previously known Hyades candidates, and the probabilities from Table 4 (without the inclusion of photometric distances) for new candidates from this work. We chose a high threshold for BANYAN Σ probabilities to investigate color trends for the most likely substellar Hyades members and to mitigate the influence of potential interlopers. There are 25 objects that survive this BANYAN Σ probability cut, including PSO J049.1159+26.8409 (W. M. J. Best et al. 2015; Z. Zhang et al. 2021); PSO J052.2746 +13.3754 and PSO J069.7303+04.3834 (W. M. J. Best et al. 2020; Z. Zhang et al. 2021); WISEA J041232.77+104408.3, WISEA J043642.75+190134.8, and WISEA J044105.56 +213001.5 (A. C. Schneider et al. 2017); Hya11 (E. Hogan et al. 2008; E. L. Martín et al. 2018), 2MASS J04183483 +2131275 (A. Pérez-Garrido et al. 2017); 2MASS J04241856 +0637448 (A. Pérez-Garrido et al. 2018); CWISE J033817.87 +171744.1, CWISE J041953.55+203628.0, CWISE J042731.38 +074344.9, and CWISE J043018.70+105857.1 (A. C. Schneider et al. 2022); CFHT-Hy-20 (J. Bouvier et al. 2008); Hya08, Hya09, Hya10, and Hya12 (E. Hogan et al. 2008; N. Lodieu et al. 2014); and CWISE J041259.89+085049.6, CWISE J042222.17

^a dist_{phot}, dist_{cp}, and dist_{BANYAN} are the photometric distance estimate, the distance predicted from the convergent point method (assuming Hyades membership), and the BANYAN Σ predicted distance (again, assuming Hyades membership), respectively.

 $[\]theta_n$ and θ_{co} are the proper motion angle and the convergent point angle, as described in the text.

 $^{^{\}rm c}$ Hyades membership probability from BANYAN Σ that does not include a distance estimate as a constraint.

^d Hyades membership probability fro BANYAN Σ that includes the photometric distance.

Table 5
Physical Properties of New Hyades Candidates

CWISE Name	Spec. Type	T _{eff} (K)	$Mass^a$ (M_{Jup})	Mass ^b (M _{Jup})
J041259.89+085049.6	T3pec (red)	1202 ± 81	35 ± 3	31+9
J042222.17+213900.5	L5-L7 (red)	1515 ± 165	47 ± 6	52 ± 7
J042356.23+130414.3	T5	1136 ± 115	33 ± 4	28^{+7}_{-4}
J043511.26+213846.3	L7.5	1378 ± 140	42 ± 5	46^{+6}_{-12}
J044116.07+143645.4	T2	1220 ± 80	35 ± 3	32^{+10}_{-4}
J044354.22+125736.7	L9pec (red)	1275 ± 81	38 ± 3	39^{+7}_{-8}
J045800.69+100456.9	T2pec (red)	1220 ± 81	35 ± 3	32^{+10}_{-4}
J051215.86+165818.0	L9	1275 ± 80	38 ± 3	39^{+7}_{-8}

Notes.

+213900.5, CWISE J042356.23+130414.3, CWISE J043511.26 +213846.3, CWISE J044116.07+143645.4, CWISE J044354.22 +125736.7, and CWISE J045800.69+100456.9 from this work.

Every candidate L- and T-type Hyades member in this sample, spanning spectral types L0.5 to T5, has a redder J-K color than the median field-age color for that spectral type, with one exception, the T3 dwarf CWISE J043018.70+105857.1 (A. C. Schneider et al. 2022). The color difference seen for the vast majority of the Hyades candidate sample compared to the field sequence may be due to several factors, including slightly lower surface gravities, enhanced metallicity, viewing angle, and variability.

Using the C. V. Morley et al. (2024) hybrid-grav evolutionary models, we find that Hyades-age brown dwarfs have $\log(g)$ values ~ 0.08 dex and ~ 0.13 dex lower than 2 Gyr and 5 Gyr objects on average, respectively, for masses between 0.03 and 0.07 M_{\odot} . While minor, this difference in surface gravity could lead to reduced absorption from collisionally induced H₂ (e.g., J. L. Linsky 1969), higher-altitude clouds (e.g., N. Madhusudhan et al. 2011), and cloud grain-size or composition differences (e.g., G. Suárez & S. Metchev 2023).

The metallicity for the Hyades has consistently been determined to be slightly metal-rich ([Fe/H] = 0.09-0.24; L. Dutra-Ferreira et al. 2016; J. D. Cummings et al. 2017; S. Gossage et al. 2018; F. Wanderley et al. 2023). Trends have been shown to exist between metallicity and infrared color excess (e.g., D. L. Looper et al. 2008; R. Zhang et al. 2024), with higher-metallicity L-type brown dwarfs having redder colors on average than those brown dwarfs with metallicities closer to solar. Though the impact of metallicity on the atmospheres of relatively cloud-free T-type brown dwarfs is unclear. However, the Diamondback models can again help to provide some insight with three different metallicities (-0.5,0.0, +0.5) available in that grid. Using synthetic photometry, we find the average J - K color difference between [M/ [H] = +0.5 and [M/H] = 0.0 models to be 0.12 mag for substellar objects with $\log(g) = 5.0$, $f_{\rm sed} = 3$, and $T_{\rm eff}$ values between 1200 K and 2200 K. Therefore, the Diamondback models support the empirical metallicity versus color trends, with higher-metallicity objects having redder near-infrared colors.

Further, whether a brown dwarf is viewed closer to edge-on or pole-on can also affect near-infrared colors (e.g., J. M. Vos

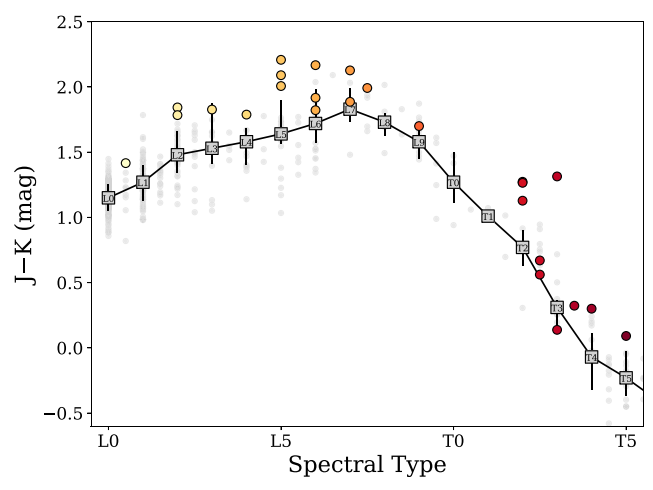


Figure 6. Color vs. near-infrared spectral type diagram for L and T dwarfs from the UHS survey in A. C. Schneider et al. (2023; gray circles) compared to candidate and confirmed Hyades L and T dwarfs (colored circles). Median colors for each spectral type for field-age objects are labeled gray squares. The error bars on the median values represent the 16 and 84 percentile ranges as determined in A. C. Schneider et al. (2023).

et al. 2017; M. E. Guerra Toro et al. 2022; G. Suárez et al. 2023). While spin alignment for stellar members has been found in some clusters (e.g., E. Corsaro et al. 2017), other inclination studies of open clusters have found that the alignment of rotation axes is not ubiquitous (e.g., R. J. Jackson & R. D. Jeffries 2010; B. F. Healy et al. 2023). Such a study of the stellar and substellar population of the Hyades would help to determine the influence of viewing angle on the observed J - K color offset for substellar Hyades members.

Lastly, variability (e.g., A. Ashraf et al. 2022; N. Oliveros--Gomez et al. 2022) and unresolved binarity (e.g., A. J. Burgasser et al. 2010; T. J. Dupuy & M. C. Liu 2012) can also affect near-infrared colors, which we showed is the potential reason for the unusually red spectra of CWISE J041259.89+085049.6 and CWISE J045800.69+100456.9 in Section 4.1. Brown dwarf binary fractions are 10%-20% for field-age objects (A. J. Burgasser et al. 2006b; J. Radigan et al. 2013; M. Aberasturi et al. 2014; C. Fontanive et al. 2018, 2023), but are much higher at young ages (M. De Furio et al. 2022). The binary fraction of Hyades-age brown dwarfs is currently unknown, but unresolved binarity could also contribute to the observed J - K color excess. We note that two of the highprobability Hyades members from Z. Zhang et al. 2021 (PSO J049.1159+26.8409 and PSO J069.7303+04.3834) were found to be strong binary candidates, while CFHT-Hy-20 (J. Bouvier et al. 2008) was found to be a weak binary candidate in that work.

Additional observations of these candidates, including highresolution imaging, variability monitoring, and/or James Webb Space Telescope spectra of silicate features in the mid-infrared (e.g., B. E. Miles et al. 2023) could help to shed light on the impact of binarity and cloud properties of these intermediateage brown dwarfs.

6. Summary

We have presented eight new candidate substellar Hyades members with spectral types ranging from L6 to T5. The positions, proper motions, and distance estimates of all eight candidates are supportive of Hyades membership, with parallax

^a Masses determined using the models of M. W. Phillips et al. (2020) and updated equation of state in G. Chabrier et al. (2023).

^b Masses determined using the hybrid-grav models of C. V. Morley et al. (2024).

and radial velocity measurements needed for full confirmation. If confirmed, CWISE J042356.23+130414.3 would be the latest spectral type, and thus lowest-mass free-floating member of the Hyades yet discovered. We find that two objects (CWISE J041259.89+085049.6 and CWISE J045800.69+100456.9) have spectra suggestive of near-infrared variability. An investigation of the near-infrared colors of the highest-probability Hyades candidates reveals that their near-infrared J-K colors are almost always redder than field-age objects of the same spectral type, potentially due to lower surface gravities and enhanced metallicity.

The primary limitation of this survey was the requirement that J-band magnitudes be brighter than 18 mag. Using the absolute J-band versus spectral type relations for UHS photometry from A. C. Schneider et al. (2023) shows that a magnitude limit of 18 can detect L5, T0, and T5 type brown dwarfs out to ~ 80 pc, ~ 52 pc, and ~ 49 pc, respectively. Note, however that the red colors of Hyades members discussed in Section 5 suggests that these distance limits are potentially upper limits. Assuming the Hyades is roughly spherical with a tidal radius of 18 pc and an average distance of 47.9 pc (Gaia Collaboration et al. 2021), the 18 mag distance limits suggest that we could be complete at spectral type L5, but are only reaching out to the approximate middle of the cluster distance for T dwarfs. The 5σ point source sensitivity of UHS survey Jband observations is 19.6 mag (S. Dye et al. 2018). Extending this type of search to the UHS J-band limit results in distance limits of \sim 159 pc for L5 dwarfs, \sim 103 pc for T0 dwarfs, and \sim 97 pc for T5 dwarfs. However, while we did not enforce a strict K-band limit, surveys for new later-type brown dwarfs in the Hyades may be limited by K-band photometry rather than J, as brown dwarfs beyond the L/T transition trend toward bluer J - K colors. Using a 5σ point source sensitivity K-band limit of 18.4 mag (J. Bruursema et al. 2024, in preparation), we find limits of \sim 204 pc, \sim 103 pc, and \sim 53 pc for L5, T0, and T5 dwarfs, respectively. Regardless, pushing this type of survey to deeper limits available with UHS would help to create a more complete census of brown dwarfs in the Hyades, especially at later spectral types (\geqslant T0).

Acknowledgments

The authors wish to thank Caroline Morley for making available the Sonora Diamondback models. This publication makes use of data products from the UKIRT Hemisphere Survey, which is a joint project of the United States Naval Observatory, the University of Hawaii Institute for Astronomy, the Cambridge University Cambridge Astronomy Survey Unit, and the University of Edinburgh Wide-Field Astronomy Unit (WFAU). This project was primarily funded by the United States Navy. The WFAU gratefully acknowledges support for this work from the Science and Technology Facilities Council through ST/T002956/1 and previous grants.

This work is based on observations obtained at the international Gemini Observatory, a program of NSF's NOIRLab, which is managed by the Association of Universities for Research in Astronomy (AURA) under a cooperative agreement with the National Science Foundation on behalf of the Gemini Observatory partnership: the National Science Foundation (United States), National Research Council (Canada), Agencia Nacional de Investigación y Desarrollo (Chile), Ministerio de Ciencia, Tecnología e Innovación (Argentina), Ministério da Ciência, Tecnología, Inovações e

Comunicações (Brazil), and Korea Astronomy and Space Science Institute (Republic of Korea).

This publication makes use of data products from the Widefield Infrared Survey Explorer, which is a joint project of the University of California, Los Angeles, and the Jet Propulsion Laboratory/California Institute of Technology, and NEOWISE, which is a project of the Jet Propulsion Laboratory/California Institute of Technology. WISE and NEOWISE are funded by the National Aeronautics and Space Administration. Part of this research was carried out at the Jet Propulsion Laboratory, California Institute of Technology, under a contract with the National Aeronautics and Space Administration.

The Pan-STARRS1 Surveys (PS1) and the PS1 public science archive have been made possible through contributions by the Institute for Astronomy, the University of Hawaii, the Pan-STARRS Project Office, the Max-Planck Society and its participating institutes, the Max Planck Institute for Astronomy, Heidelberg and the Max Planck Institute for Extraterrestrial Physics, Garching, The Johns Hopkins University, Durham University, the University of Edinburgh, the Queen's University Belfast, the Harvard-Smithsonian Center for Astrophysics, the Las Cumbres Observatory Global Telescope Network Incorporated, the National Central University of Taiwan, the Space Telescope Science Institute, the National Aeronautics and Space Administration under grant No. NNX08AR22G issued through the Planetary Science Division of the NASA Science Mission Directorate, the National Science Foundation grant No. AST-1238877, the University of Maryland, Eotvos Lorand University (ELTE), the Los Alamos National Laboratory, and the Gordon and Betty Moore Foundation.

This work has benefitted from The UltracoolSheet at http://bit.ly/UltracoolSheet, maintained by Will Best, Trent Dupuy, Michael Liu, Aniket Sanghi, Rob Siverd, and Zhoujian Zhang, and developed from compilations by T. J. Dupuy & M. C. Liu (2012), T. J. Dupuy & A. L. Kraus (2013), N. R. Deacon et al. (2014), M. C. Liu et al. (2016), W. M. J. Best et al. (2018, 2021), A. C. Schneider et al. (2023), and A. Sanghi et al. (2023).

The authors wish to recognize and acknowledge the very significant cultural role and reverence that the summit of Maunakea has always had within the indigenous Hawaiian community. We are most fortunate to have the opportunity to conduct observations from this mountain.

Software: BANYAN Σ (J. Gagné et al. 2018), pypeit (J. Prochaska et al. 2020; J. X. Prochaska et al. 2023).

ORCID iDs

Adam C. Schneider https://orcid.org/0000-0002-6294-5937 Michael C. Cushing https://orcid.org/0000-0001-7780-3352 Robert A. Stiller https://orcid.org/0000-0002-7181-2554 Jeffrey A. Munn https://orcid.org/0000-0002-4603-4834 Justice Bruursema https://orcid.org/0000-0002-3858-1205 Michael C. Liu https://orcid.org/0000-0003-2232-7664 Alexia Bravo https://orcid.org/0009-0002-3936-8059 Jacqueline K. Faherty https://orcid.org/0000-0001-6251-0573

Austin Rothermich https://orcid.org/0000-0003-4083-9962 Emily Calamari https://orcid.org/0000-0002-2682-0790 Dan Caselden https://orcid.org/0000-0001-7896-5791 Martin Kabatnik https://orcid.org/0000-0003-4905-1370 Arttu Sainio https://orcid.org/0000-0003-4864-5484 Thomas P. Bickle https://orcid.org/0000-0003-2235-761X

Nikolaj Stevnbak Andersen https://orcid.org/0000-0003-4714-3829

Melina Thévenot https://orcid.org/0000-0001-5284-9231

References

```
Aberasturi, M., Burgasser, A. J., Mora, A., et al. 2014, AJ, 148, 129
Allers, K. N., & Liu, M. C. 2013, ApJ, 772, 79
Ashraf, A., Bardalez Gagliuffi, D. C., Manjavacas, E., et al. 2022, ApJ,
   934, 178
Bannister, N. P., & Jameson, R. F. 2007, MNRAS, 378, L24
Bardalez Gagliuffi, D. C., Burgasser, A. J., Gelino, C. R., et al. 2014, ApJ,
   794, 143
Bell, C. P. M., Mamajek, E. E., & Naylor, T. 2015, MNRAS, 454, 593
Best, W. M. J., Liu, M. C., Magnier, E. A., et al. 2015, ApJ, 814, 118
Best, W. M. J., Magnier, E. A., Liu, M. C., et al. 2018, ApJS, 234, 1
Best, W. M. J., Liu, M. C., Magnier, E. A., et al. 2020, AJ, 159, 257
Best, W. M. J., Liu, M. C., Magnier, E. A., et al. 2021, AJ, 161, 42
Boss, L. J. 1908, AJ, 26, 31
Bouvier, J., Kendall, T., Meeus, G., et al. 2008, A&A, 481, 661
Brandt, T. D., & Huang, C. X. 2015a, ApJ, 807, 24
Brandt, T. D., & Huang, C. X. 2015b, ApJ, 807, 58
Bravo, A., Schneider, A. C., Bardalez Gagliuffi, D., et al. 2023, AJ, 166, 226
Bryja, C., Jones, T. J., Humphreys, R. M., et al. 1992, ApJL, 388, L23
Bryja, C., Humphreys, R. M., & Jones, T. J. 1994, AJ, 107, 246
Burgasser, A. J., Kirkpatrick, J. D., Brown, M. E., et al. 2002, ApJ, 564, 421
Burgasser, A. J., McElwain, M. W., Kirkpatrick, J. D., et al. 2004, AJ,
   127, 2856
Burgasser, A. J., Geballe, T. R., Leggett, S. K., et al. 2006a, ApJ, 637, 1067
Burgasser, A. J., Kirkpatrick, J. D., Cruz, K. L., et al. 2006b, ApJS, 166, 585
Burgasser, A. J. 2007, ApJ, 659, 655
Burgasser, A. J., Cruz, K. L., Cushing, M., et al. 2010, ApJ, 710, 1142
Burrows, A., Marley, M., Hubbard, W. B., et al. 1997, ApJ, 491, 856
Canty, J. I., Lucas, P. W., Roche, P. F., & Pinfield, D. J. 2013, MNRAS,
   435, 2650
Casewell, S. L., Littlefair, S. P., Burleigh, M. R., & Roy, M. 2014, MNRAS,
   441, 2644
Chambers, K. C., Magnier, E. A., Metcalfe, N., et al. 2016, arXiv:1612.05560
Chabrier, G., Baraffe, I., Phillips, M., et al. 2023, A&A, 671, A119
Corsaro, E., Lee, Y.-N., García, R. A., et al. 2017, NatAs, 1, 0064
Cummings, J. D., Deliyannis, C. P., Maderak, R. M., et al. 2017, AJ, 153, 128
Deacon, N. R., Liu, M. C., Magnier, E. A., et al. 2014, ApJ, 792, 119
de Bruijne, J. H. J., Hoogerwerf, R., & de Zeeuw, P. T. 2001, A&A, 367, 111
De Furio, M., Liu, C., Meyer, M. R., et al. 2022, ApJ, 941, 161
De Gennaro, S., von Hippel, T., Jefferys, W. H., et al. 2009, ApJ, 696, 12
Dobbie, P. D., Kenyon, F., Jameson, R. F., et al. 2002, MNRAS, 329, 543
Dupuy, T. J., & Liu, M. C. 2012, ApJS, 201, 19
Dupuy, T. J., & Kraus, A. L. 2013, Sci, 341, 1492
Dutra-Ferreira, L., Pasquini, L., Smiljanic, R., et al. 2016, A&A, 585, A75
Dye, S., Lawrence, A., Read, M. A., et al. 2018, MNRAS, 473, 5113
Elias, J. H., Joyce, R. R., Liang, M., et al. 2006, Proc. SPIE, 6269, 62694C
Faherty, J. K., Riedel, A. R., Cruz, K. L., et al. 2016, ApJS, 225, 10
Fontanive, C., Biller, B., Bonavita, M., & Allers, K. 2018, MNRAS, 479, 2702
Fontanive, C., Bedin, L. R., De Furio, M., et al. 2023, MNRAS, 526, 1783
Franson, K., Bowler, B. P., Bonavita, M., et al. 2023, AJ, 165, 39
Gagné, J., Mamajek, E. E., Malo, L., et al. 2018, ApJ, 856, 23
Gaia Collaboration, Smart, R. L., Sarro, L. M., et al. 2021, A&A, 649, A6
Gaia Collaboration, Vallenari, A., Brown, A. G. A., et al. 2023, A&A, 674, A1
Giclas, H. L., Burnham, R., & Thomas, N. G. 1962, LowOB, 5, 257
Gizis, J. E., Reid, I. N., & Monet, D. G. 1999, AJ, 118, 997
Goldman, B., Röser, S., Schilbach, E., et al. 2013, A&A, 559, A43
Gossage, S., Conroy, C., Dotter, A., et al. 2018, ApJ, 863, 67
Guerra Toro, M. E., Zhou, Y., & Bowler, B. P. 2022, RNAAS, 6, 250
Hanson, R. B. 1975, AJ, 80, 379
Harris, H. C., Vrba, F. J., Dahn, C. C., et al. 1999, AJ, 117, 339
Hayashi, C., & Nakano, T. 1963, PThPh, 30, 460
Healy, B. F., McCullough, P. R., Schlaufman, K. C., et al. 2023, ApJ, 944, 39
Herbig, G. H. 1962, ApJ, 135, 736
Hertzsprung, E. 1921, Bull. Astron. Inst. Netherlands, 1, 4
Hodierna, G. B. 1654, De systemate orbis cometici deque admirandis coeli
   characteribus, opuscula duo, in quorum primo cometarum causae
   disquiruntur, & explicantur, necnon vie Com etarum, per orbem
   cometicum multiplices indicantur. In secundo vero quid, quales, quotue
   sint stellae luminosae, nebulae, necnon, & occultae, manifestantur & rerum
   caelestium studiosis commendantur (Zürich: ETH-Bibliothek Zürich), 1654
```

```
Hogan, E., Jameson, R. F., Casewell, S. L., Osbourne, S. L., & Hambly, N. C.
  2008, MNRAS, 388, 495
Irwin, M. J., Lewis, J., Hodgkin, S., et al. 2004, Proc. SPIE, 5493, 411
Jackson, R. J., & Jeffries, R. D. 2010, MNRAS, 402, 1380
Johnson, H. L., & Knuckles, C. F. 1955, ApJ, 122, 209
Kapteyn, J. C., & Desetter, W. 1904, PGro, 14, I-87
Kirkpatrick, J. D., Reid, I. N., Liebert, J., et al. 1999, ApJ, 519, 802
Kirkpatrick, J. D., Reid, I. N., Liebert, J., et al. 2000, AJ, 120, 447
Kirkpatrick, J. D., Looper, D. L., Burgasser, A. J., et al. 2010, ApJS, 190, 100
Kirkpatrick, J. D., Cushing, M. C., Gelino, C. R., et al. 2011, ApJS, 197, 19
Kirkpatrick, J. D., Gelino, C. R., Faherty, J. K., et al. 2021, ApJS, 253, 7
Kuchner, M. J., Faherty, J. K., Schneider, A. C., et al. 2017, ApJL, 841, L19
Kumar, S. S. 1963, ApJ, 137, 1121
Kustner, F. 1902, AN, 158, 359
Kuzuhara, M., Currie, T., Takarada, T., et al. 2022, ApJL, 934, L18
Lawrence, A., Warren, S. J., Almaini, O., et al. 2007, MNRAS, 379, 1599
Lebreton, Y., Fernandes, J., & Lejeune, T. 2001, A&A, 374, 540
Leggett, S. K., & Hawkins, M. R. S. 1989, MNRAS, 238, 145
Leggett, S. K., Harris, H. C., & Dahn, C. C. 1994, AJ, 108, 944
Leggett, S. K., Geballe, T. R., Fan, X., et al. 2000, ApJL, 536, L35
Linsky, J. L. 1969, ApJ, 156, 989
Liu, M. C., Dupuy, T. J., & Allers, K. N. 2016, ApJ, 833, 96
Lodieu, N., Boudreault, S., & Bejar, V. J. S. 2014, MNRAS, 445, 3908
Lodieu, N., Smart, R. L., Pérez-Garrido, A., et al. 2019, A&A, 623, A35
Lodieu, N. 2020, Mem. Soc. Astron. Italiana, 91, 84
Looper, D. L., Kirkpatrick, J. D., Cutri, R. M., et al. 2008, ApJ, 686, 528
Lucas, P. W., Hoare, M. G., Longmore, A., et al. 2008, MNRAS, 391, 136
Luyten, W. J., & Merrill, P. W. 1954, PASP, 66, 207
Madhusudhan, N., Burrows, A., & Currie, T. 2011, ApJ, 737, 34
Madsen, S., Dravins, D., & Lindegren, L. 2002, A&A, 381, 446
Magnier, E. A., Schlafly, E. F., Finkbeiner, D. P., et al. 2020, ApJS, 251, 6
Marley, M. S., Saumon, D., Visscher, C., et al. 2021, ApJ, 920, 85
Marocco, F., Day-Jones, A. C., Lucas, P. W., et al. 2014, MNRAS, 439, 372
Marocco, F., Eisenhardt, P. R. M., Fowler, J. W., et al. 2021, ApJS, 253, 8
Martín, E. L., Lodieu, N., Pavlenko, Y., et al. 2018, ApJ, 856, 40
Meingast, S., & Alves, J. 2019, A&A, 621, L3
Melnikov, S., & Eislöffel, J. 2018, A&A, 611, A34
Miles, B. E., Biller, B. A., Patapis, P., et al. 2023, ApJL, 946, L6
Morley, C. V., Mukherjee, S., Marley, M. S., et al. 2024, arXiv:2402.00758
Oliveros-Gomez, N., Manjavacas, E., Ashraf, A., et al. 2022, ApJ, 939, 72
Oort, J. H. 1979, A&A, 78, 312
Pels, G., Oort, J. H., & Pels-Kluyver, H. A. 1975, A&A, 43, 423
Pérez-Garrido, A., Lodieu, N., & Rebolo, R. 2017, A&A, 599, A78
Pérez-Garrido, A., Lodieu, N., Rebolo, R., et al. 2018, A&A, 620, A130
Perryman, M. A. C., Brown, A. G. A., Lebreton, Y., et al. 1998, A&A, 331, 81
Pesch, P. 1968, ApJ, 151, 605
Phillips, M. W., Tremblin, P., Baraffe, I., et al. 2020, A&A, 637, A38
Prochaska, J., Hennawi, J., Westfall, K., et al. 2020, JOSS, 5, 2308
Prochaska, J. X., Hennawi, J., Cooke, R., et al. 2023, Zenodo
Proctor, R. A. 1870, RSPS, 18, 169
Radigan, J., Jayawardhana, R., Lafrenière, D., et al. 2012, ApJ, 750, 105
Radigan, J., Jayawardhana, R., Lafrenière, D., et al. 2013, ApJ, 778, 36
Ramberg, J. M. 1941, StoAn, 13, 9.1
Reid, N. 1992, MNRAS, 257, 257
Reid, N. 1993, MNRAS, 265, 785
Reid, I. N., & Gizis, J. E. 1997, AJ, 114, 1992
Reid, I. N., & Hawley, S. L. 1999, AJ, 117, 343
Reid, I. N., & Mahoney, S. 2000, MNRAS, 316, 827
Reid, I. N., Lewitus, E., Burgasser, A. J., et al. 2006, ApJ, 639, 1114
Reino, S., de Bruijne, J., Zari, E., d'Antona, F., & Ventura, P. 2018, MNRAS,
  477, 3197
Röser, S., Schilbach, E., Piskunov, A. E., et al. 2011, A&A, 531, A92
Röser, S., Schilbach, E., & Goldman, B. 2019, A&A, 621, L2
Sanghi, A., Liu, M. C., Best, W. M., et al. 2023, ApJ, 959, 63
Saumon, D., & Marley, M. S. 2008, ApJ, 689, 1327
Schneider, A. C., Cushing, M. C., Kirkpatrick, J. D., et al. 2014, AJ, 147, 34
Schneider, A. C., Windsor, J., Cushing, M. C., et al. 2017, AJ, 153, 196
Schneider, A. C., Vrba, F. J., Munn, J. A., et al. 2022, AJ, 163, 242
Schneider, A. C., Munn, J. A., Vrba, F. J., et al. 2023, AJ, 166, 103
Skrutskie, M. F., Cutri, R. M., Stiening, R., et al. 2006, AJ, 131, 1163
Suárez, G., & Metchev, S. 2023, MNRAS, 523, 4739
Suárez, G., Vos, J. M., Metchev, S., et al. 2023, ApJL, 954, L6
Stauffer, J. 1982, AJ, 87, 899
Stauffer, J. R., Liebert, J., Giampapa, M., et al. 1994, AJ, 108, 160
Stauffer, J. R., Liebert, J., & Giampapa, M. 1995, AJ, 109, 298
Taylor, B. J. 2006, AJ, 132, 2453
Titus, J., & Morgan, W. W. 1940, ApJ, 92, 256
```

```
Upgren, A. R., & Weis, E. W. 1977, AJ, 82, 978 van Altena, W. F. 1966, AJ, 71, 482 van Altena, W. F. 1969, AJ, 74, 2 van Bueren, H. G. 1952, Bull. Astron. Inst.Netherlands, 11, 385 van Maanen, A. 1942, PASP, 54, 109 van Rhijn, P. J., & Raimond, J. J. 1934, MNRAS, 94, 508 Vos, J. M., Allers, K. N., & Biller, B. A. 2017, ApJ, 842, 78
```

```
Wanderley, F., Cunha, K., Souto, D., et al. 2023, ApJ, 951, 90 Weersman, H. A. 1904, PGro, 13, 1 Wilson, R. E. 1948, ApJ, 107, 119 Wirtz, C. W. 1902, AN, 160, 17 Zhang, Z., Liu, M. C., Best, W. M. J., et al. 2021, ApJ, 911, 7 Zhang, R., Liu, M. C., & Zhang, Z. 2024, ApJ, 960, 105 Zuckerman, B., & Becklin, E. E. 1987, ApJL, 319, L99
```